



# Study of optical and electrical property of NaI-doped PPy thin film with excellent photocatalytic property at visible light

Srimathi Krishnaswamy<sup>1</sup> · Veena Ragupathi<sup>1</sup> · Sudarkodi Raman<sup>1</sup> · Puspamitra Panigrahi<sup>1</sup> · Ganapathi Subramaniam Nagarajan<sup>2</sup>

Received: 3 June 2018 / Revised: 27 November 2018 / Accepted: 7 December 2018 /  
Published online: 11 December 2018  
© Springer-Verlag GmbH Germany, part of Springer Nature 2018

## Abstract

Conductive polymers perform as a new class of very active photocatalysts under visible light. Among them, polypyrrole (PPy) is one of the most promising conjugated polymers with a wide range of applications. PPy and doped PPy were synthesized on glass plate in thin film form by a facile simple successive ionic layer adsorption and reaction method. Polypyrrole is doped with dodecyl benzene sulphonic acid, toluene sulphonic acid, hydrochloric acid, sodium iodide (NaI), citric acid (commercial) and citric acid (lemon). The synthesized thin film was well characterized using UV–visible spectrophotometer, scanning electron microscopy, Fourier transform infrared spectroscopy, thermogravimetric analysis and photoluminescence (PL). The electrical conductivity was measured by Hall effect measurements. Among various organic and inorganic acid dopants, NaI-doped PPy thin film exhibited narrow band gap and has excellent ability to absorb light in red region of the spectrum. NaI-doped PPy thin film showed higher conductivity when compared to other dopants. A lower PL intensity of NaI-PPy thin film indicates higher electron–hole pair separation efficiency. The photocatalytic activities of PPy thin film and NaI-doped PPy thin film on rhodamine 6G dye under visible light were systematically investigated. NaI-doped PPy thin film had better degradation efficiency than PPy due to its higher electron–hole pair separation efficiency.

**Keywords** Polypyrrole · Thin film · Dye degradation · Rhodamine 6G

✉ Srimathi Krishnaswamy  
ksrimathi@hindustanuniv.ac.in

✉ Ganapathi Subramaniam Nagarajan  
ganapathi@dongguk.edu

<sup>1</sup> Centre for Clean Energy and Nano Convergence (CENCON), Hindustan Institute of Technology and Science (HITS), Padur, Kelambakkam, Chennai 603103, India

<sup>2</sup> Quantum Functional Semiconductor Research Centre (QSRC), Nano Information Technology Academy (NITA), Dongguk University, 26 phildong3-ga, Chung-gu, Seoul 100-715, Korea

## Introduction

The development of efficient and environmentally friendly approaches for energy conversion and storage is one of the vital challenges of the twenty-first century [1]. Nanomaterials potentially provide paradigm-changing solutions to energy conversion processes that occur at surfaces [2, 3]. Titanium dioxide ( $\text{TiO}_2$ ) is currently the most widely used photocatalyst because of its high photocatalytic activity, stability, low cost and non-toxicity. Nevertheless,  $\text{TiO}_2$  applications are limited because of a low quantum yield with the fast charge carriers ( $e^-/h^+$ ) recombination and the necessity to use UV irradiation. In fact,  $\text{TiO}_2$  can only be excited by UV irradiation and it absorbs only 3–4% of the solar light [4–6]. In the last few years, a considerable number of novel strategies including doping, heterojunctions, graphene-based composition and co-catalyst have been proposed to offer new photocatalytic materials as potential substitutes of  $\text{TiO}_2$  for the most relevant photocatalytic applications such as detoxification and disinfection, water splitting and organic synthesis [7–9]. To achieve high visible-light-induced photocatalytic activity, it is essential to fine-tune several electronic characteristics of photocatalysts such as band gap energy, band position, lifetime of electrons and holes [9, 10]. Several methods, including the use of dopants such as carbon or nitrogen, have been used to reduce the band gap of  $\text{TiO}_2$ .

Recently, black hydrogenated  $\text{TiO}_2$  nanocrystals with high photocatalytic activity under solar light have been developed [11]. Linic and Weng reported that plasmonic photocatalysts have appeared as a very promising way to improve the activity of  $\text{TiO}_2$  in the visible light [12, 13]. Moreover, surface modification of  $\text{TiO}_2$  with Cu, Ag or Au nanoparticles significantly enhances the photocatalytic activity under UV and visible light [14–16]. However, the high cost of the noble metal-doped catalyst (i.e. Au, Ag) and the low stability with repeated cycling significantly limit their large-scale applications [17]. Hence, the existing photocatalysts have not yet found the way for practical applications. In the last few years, polymer nanostructures have attracted a lot of attention for energy conversion and storage applications [18].

Among all conducting polymers, polypyrrole (PPy) is one of the most promising conducting polymers because of its excellent thermal and chemical stability, high conductivity, low cost and elevated carrier mobility as well as biocompatibility. These unique characteristics make PPy potentially useful for a broad range of applications, including solar cells, biosensors and organic light-emitting devices [19–21]. Although oxide-based semiconductors have been in vogue as efficient photocatalysts in the past decade, the reports regarding photocatalytic activity of conjugated polymers are scarce [18, 22]. Also, many conjugated polymers act as efficient electron donors and good hole transporters upon visible-light excitation. The dopants in the conducting polymer play a significant role in determining photocatalytic and photovoltaic efficiency, since they affect both band gap and electrical conductivity. In the present work, polypyrrole is doped with dodecyl benzene sulphonic acid (DBSA), toluene sulphonic acid (TSA), hydrochloric acid (HCl), sodium iodide (NaI) citric acid (commercial) and citric acid (lemon).

To the best of our knowledge, there has been no previous study on the synthesis of NaI-doped PPy thin film by using SILAR method. We show that conducting PPy thin film and NaI-doped PPy thin film synthesized by SILAR method exhibit better photocatalytic activities in visible light.

## Experimental

### Materials

Pyrrole (Spectrochem) and ammonium persulphate (APS) (SD Fine Chemical) were used as precursors for the synthesis of undoped and doped polypyrrole. Dodecyl benzene sulphonic acid (DBSA) (SD Fine Chemical), P-toluene sulphonic acid monohydrate (PTSA) (Spectrochem), hydrochloric acid (HCl) (Merck), sodium iodide (NaI) (Merck), citric acid (Fischer Scientific) and citric acid (from citrus × lemon extract) were used as dopants.

### Synthesis of polypyrrole (PPy) thin films

Polypyrrole (PPy) thin films were deposited by a simple successive ionic layer adsorption and reaction (SILAR) method on glass plates at room temperature. The SILAR method consists of two chemical baths. One bath consists of 0.1 M (7 ml) of pyrrole in 50 ml distilled water and another bath consists of 0.2 M (4.56 g) ammonium persulphate (APS) dissolved in 50 mL of distilled water. The cleaned glass substrate was dipped into pyrrole solution for 10 s, and then, the substrate was dipped into APS solution for 10 s, the slide from the solution was removed and the glass slide was heated at 70 °C to form polypyrrole thin film. In order to prepare monomer-free thin film, the resultant films were rinsed with distilled water. Twenty cycles of coating were done to obtain the thin film. The same procedure was adopted for doped PPy by using 0.05 M of dopant. The synthesized PPy with DBSA, PTSA, HCl, NaI, citric acid and citric acid (from citrus x lemon extract) labelled as DBSA-PPy, Toly-PPy, HCl-PPy, NaI-PPy, C1-PPy and C2-PPy, respectively, was characterized. The chemical reaction for formation of PPy is depicted in Fig. 1a. The schematic representation for synthesis of PPy thin film by SILAR method is depicted in Fig. 1b.

### Characterization

UV absorbance studies were performed by UV–visible spectrophotometer (Shimadzu double-beam monochromator spectrophotometer (UV-2540)). The morphology of the synthesized composite films was investigated by using SEM (FESEM S-4800Hitachi Model Scanning Electron Microscope). Fourier transform infrared (FTIR) spectra were recorded on JASCO model 6300. Thermal properties were obtained by TGA (PerkinElmer model TGA 7) in the range 20–800 °C at 2 °C/min in nitrogen atmosphere. The DC electric measurements were taken by Ecopia Hall

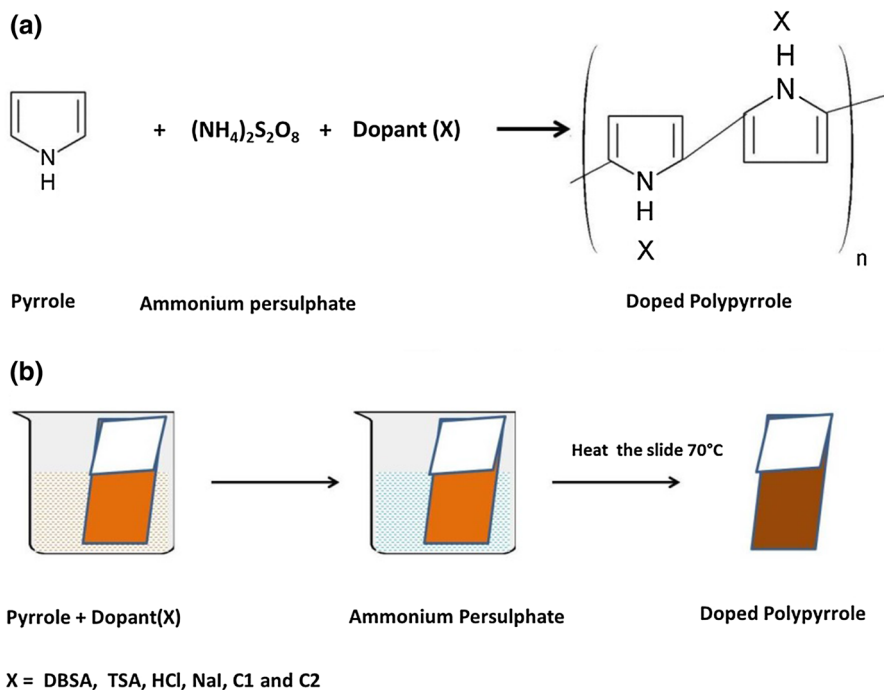


**Fig. 1** **a** Chemical reaction for formation of PPy, **b** schematic representation for synthesis of PPy thin film by SILAR method

effect Measurement system (HMS-5000). Photoluminescence (PL) studies were analysed using JASCO 8660 Spectrofluorometer. The catalytic activity of PPy and NaI-doped PPy thin film was evaluated by the total mineralization of rhodamine 6G, a basic dye in aqueous solution using a double-walled quartz photoreactor having 150 W mercury lamp as a light source supplied by SAIC, India.

### Photocatalytic activity of synthesized thin films

A 150 W mercury lamp was used as the light source. The reactor vessel was kept at 25 °C using circulated water. 1 cm × 1 cm of thin film catalyst was added to 350 ml rhodamine 6G (R6G) dye solution of 5 mg/L concentration. Prior to visible irradiation, the R6G dye solution was kept over the catalyst and stirred in the dark for 1 h to reach the sorption equilibrium. During the irradiation, about 5 mL liquid was taken from the reaction cell at regular time intervals. The dye solution was analysed by UV–Vis spectrophotometer. The absorbance of R6G was measured at 524 nm. The amount of removal of the R6G dye, in terms of percentage removal, has been calculated using the following relationship:

$$\text{Percentage removal (\%R)} = \left[ C_i - C_f / C_i \right] \times 100 \quad (1)$$

where  $C_i$  and  $C_f$  are the initial and final concentrations of dye (ppm) at a given time.

## Results and discussion

### Optical studies

Optical studies were done by using UV–visible spectrophotometer. The UV absorbance of citric acid from lemon extract and commercial citric acid is shown in Fig. 2. An absorbance peak at 288 nm is observed for lemon extract, and an absorbance peak at 282 nm is observed for commercial citric acid. Alam [23] has reported the absorbance peak at 280 nm for citrus products which well agrees with our absorbance spectra. So in our present study, lemon contains citric acid as a main ingredient which was confirmed by UV absorbance studies. The IUPAC name of citric acid is 1,2,3-propanetricarboxylic acid. The absorbance spectra are due to the presence of three carboxylic acids in citric acid. Rauf et al. [24] have reported the presence of phytochemicals in citrus lemon which are reducing sugar, tannins, flavonoids, terpenoids and phenols. After comparing with the literature, we argue that in our present study, the higher absorbance in citrus lemon is due to the presence of phytochemicals present in the bio-extract.

Figure 3 shows the UV absorption spectra of polypyrrole and doped polypyrrole thin film measured over the wavelength range of 200–900 nm. PPy thin film shows an absorbance peak at 383 nm which is attributed to  $\pi$ – $\pi^*$  electronic transition. All other doped PPy thin films exhibited a broad peak starting from 372 to 532 nm. Small shoulder peaks observed at 474 nm and 512 nm correspond to polaron transition [25, 26]. Similar type of absorbance peaks is reported in earlier literature for pure PPy thin films [26]. While NaI-PPy and C2-PPy thin film exhibits a broad peak which extends up to 700 nm, individual peaks are not visible for these polymers. All the three peaks corresponding to  $\pi$ – $\pi^*$  electronic transition, polaron and bipolaron

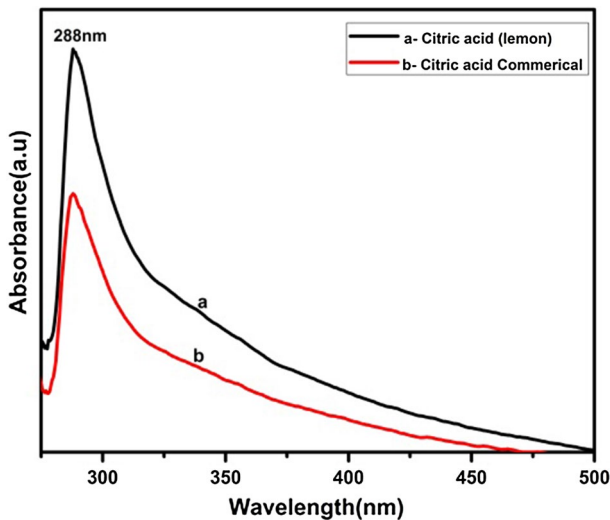
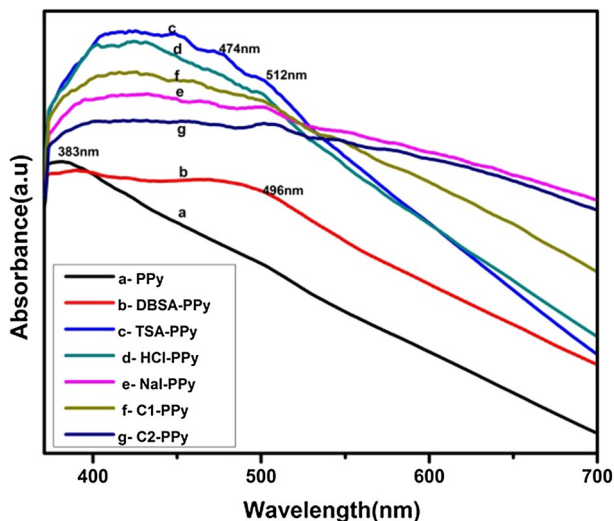


Fig. 2 UV absorbance of citric acid commercial and lemon extract



**Fig. 3** UV absorbance of PPy and doped PPy thin film

peaks merged to form broad peak covering the UV and visible part of solar spectrum. Sharp distinct absorption peaks are not visible. Instead of sharp peaks, three peaks merged to form a slope implying high concentration of  $\pi-\pi^*$  electronic transition and very less concentration of polaron and bipolaron transitions. In the case of NaI-PPy and C2-PPy thin films, a wide peak around 380–700 nm is observed, which implies the availability of more number of polarons and bipolarons when compared to other dopants. So UV–Vis absorption spectra of PPy and doped PPy confirm the formation of PPy thin film. When compared to PPy, the doped PPy exhibited red-shift due to the effect of dopants. TSA-PPy thin film shows more intense peak than other doped PPy thin film. Song et al. [27] reported that the shorter alkyl length in doped PPy, which shows the more intense peak, would result in the higher conductivity. NaI-PPy has the ability to cover the full visible light when compared to other doped PPy thin films, so we expect that this thin film will act as a better photocatalyst in dye degradation in the presence of visible light.

In the present work, thickness of the film was measured by the gravimetric weight difference method using relation,

$$t = \frac{m}{\rho \times A} \quad (2)$$

where  $m$  is the mass of the deposited film measured by sensitive microbalance;  $A$  is the area of the deposited film; and  $\rho$  is the density of the deposited materials. Table 1 shows the band gap and thickness of the thin film.

The band gap of thin film was calculated using the following equation:

$$\alpha = \frac{1}{t} \left( \frac{ln I}{T} \right) \quad (3)$$

**Table 1** Thickness and band gap PPy and doped PPy

	PPy	DBSA-PPy	TSA-PPy	HCl-PPy	NaI-PPy	C1-PPy	C2-PPy
Thickness (μm)	0.7	1.7	2.6	1.8	3.5	1.5	2.6
Band gap (eV)	2.32	2.11	1.96	1.93	1.75	1.86	1.81

where  $T$  is the transmittance and  $t$  thickness of thin film.

$$A = \log_{10} 1/T \tag{4}$$

where  $A$  is the absorbance.

The band gap of PPy and Doped PPy is shown in Fig. 4. The band gap is in the decreasing order for PPy > DBSA-PPy > TSA-PPy > HCl-PPy > C1-PPy > C2-PPy > NaI-PPy. The band gap of DSA-PPy and TSA-PPy is low when compared to PPy. This may be due to the bulky group (TSA and DBSA) present in polypyrrole, which creates polaronic and bipolaronic sublevels with in the gap. TSA-PPy shows low band gap compared to DBSA-PPy because it contains short alkyl chain group (TSA) when compared to long alkyl chain group (DBSA). The presence of three carboxylic groups in C1-PPy and C2-PPy produces more polaronic, bipolaronic sublevels with in the gap. So C1-PPy and C2-PPy have lower band gap compared to DBSA-PPy and TSA-PPy. Hazarika and Kumar [28] revealed that PPy nanofibers doped with short alkyl chain exhibited smaller optical band gap. In our present study, the NaI-PPy thin film shows the very low band gap of 1.75 eV, which falls in red region in spectrum compared to other doped PPy, which is shown in Fig. 5. This may be due to the availability of more polaronic, bipolaronic sublevels with in the gap of NaI-PPy when compared to other dopants.

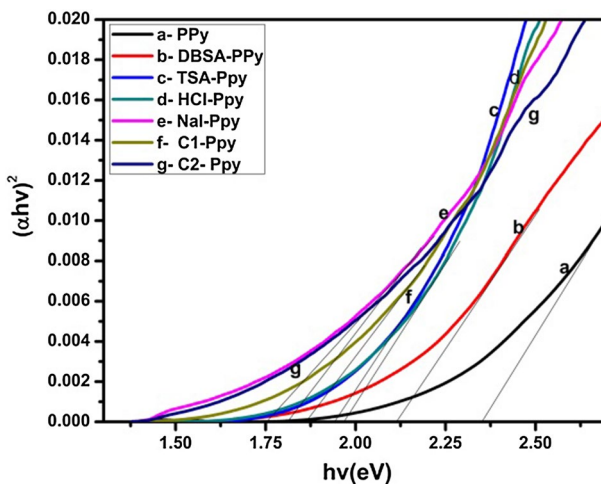


**Fig. 4** Band gap of PPy and doped PPy thin film

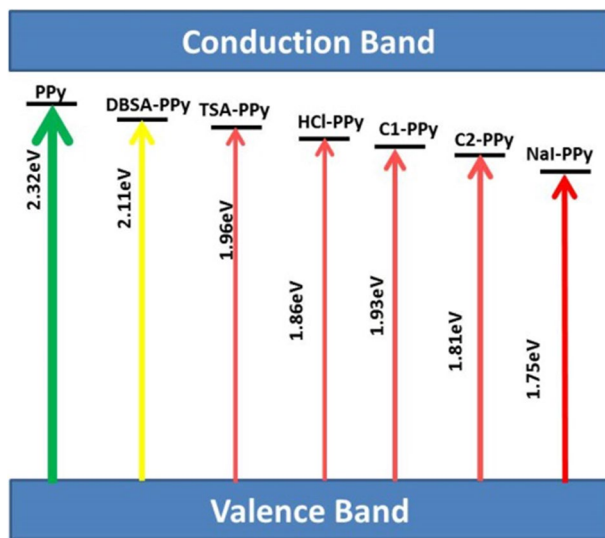


**Fig. 5** Schematic representation of PPy and doped PPy band gap position in visible part of spectrum

The energy band gap determines which wavelength(s) of light can be absorbed which in turns assists to identify the photovoltaic and photocatalytic efficiency. The poly(phenylene), poly(3-hexylthiophene) and poly(fluorene) copolymer derivatives synthesized via tedious process consumed toxic chemicals exhibited band gap from 2.00 to 2.5 eV [29], and it is chemically unstable. In our present study, we have incorporated NaI in PPy and attained the band gap of 1.75 eV which is much lower than that for the previously reported by Chen [29]. We have adopted easy and economical method of fabricating thin film compared to the literature [29], and the thin film is environmentally, chemically and electrically stable.

### Morphological analysis

The morphology of the thin film was analysed by SEM images, which is shown in Fig. 6. NaI-PPy thin film has low band gap, so it was taken further for SEM analysis. Figure 6a shows the SEM image of PPy thin film which has uniform surface but with some cracks. Figure 6b shows the SEM image of NaI-PPy thin film having doughnut-shaped grains with average grain size of 20  $\mu\text{m}$ . The cross section of PPy thin film is shown in Fig. 6c. This image reveals that the layer is uniform with thickness of 0.506  $\mu\text{m}$ . Figure 6d shows the cross-sectional view of NaI-PPy thin film. The thickness is found to be 4.102  $\mu\text{m}$  with irregular shape. The irregular shape may be due to the presence of NaI present in the polymer backbone.



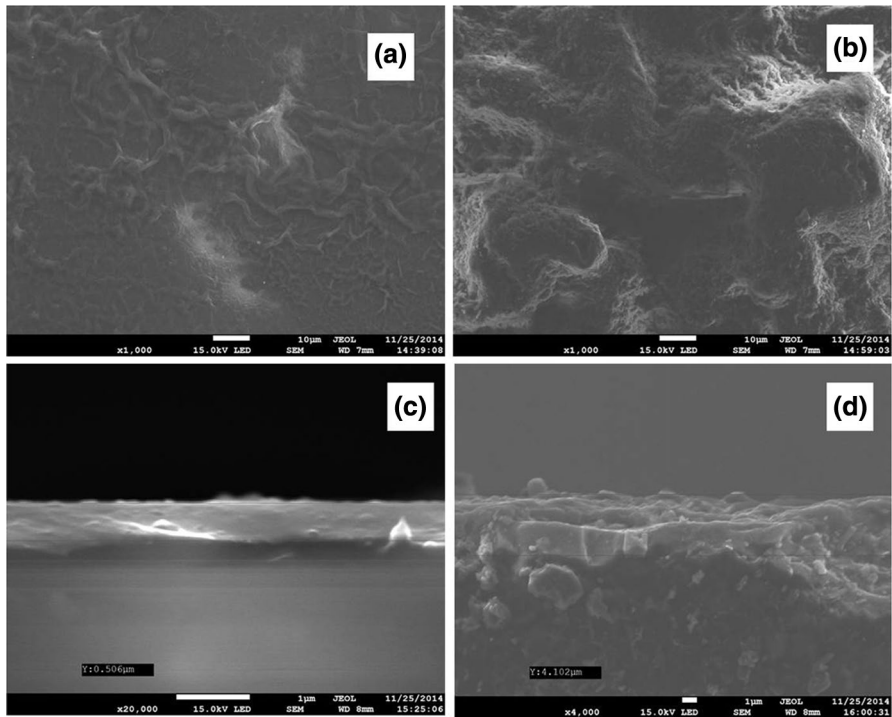


**Fig. 6** SEM of **a** PPy thin film, **b** NaI-PPy thin film, **c** cross section of PPy thin film, **d** cross section of NaI-PPy thin film

### Fourier transform infrared spectroscopy

FTIR analysis was performed to verify the functional group in the synthesized film. Figure 7 shows the FTIR spectra of polypyrrole and doped polypyrrole. The peak near  $1292\text{ cm}^{-1}$  is due to C–N stretching and C–C vibration of the polymer [30]. The pyrrole ring stretching is obtained at  $1440\text{ cm}^{-1}$ . The C=N stretching is observed at  $1672$  and  $1630\text{ cm}^{-1}$  [31]. Secondary amine (–NH) group can be recognized by absorption due to N–H stretching in the region  $3246\text{--}3560\text{ cm}^{-1}$  [32, 33] confirming the formation of PPy. The same characteristic peaks were also observed for the NaI-PPy with some shift in the wave number, as well as change in the intensity of the peaks, as compared to that of PPy. The additional peaks in respective IR spectra confirm the dopant effect in the thin film samples.

### Thermal gravimetric analysis (TGA)

Thermal studies were done by TGA. Figure 8 shows the TGA curves of PPy and doped PPy. The PPy and doped PPy follow three steps during the decomposition

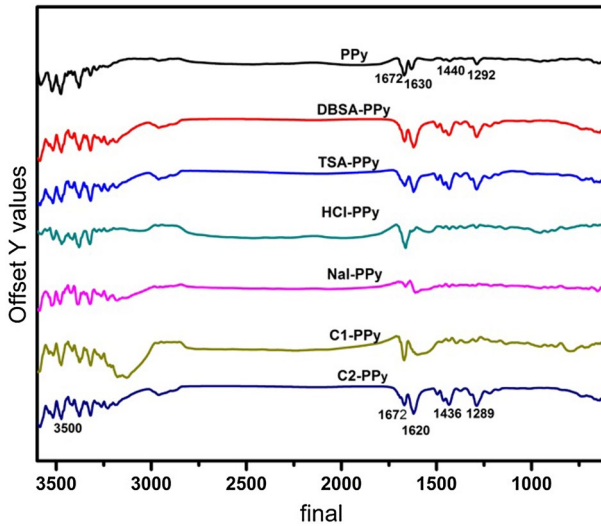


Fig. 7 FTIR image of PPy and doped PPy thin film

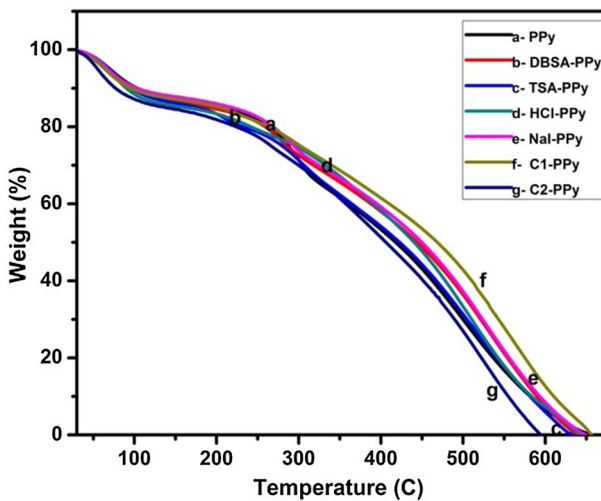


Fig. 8 Thermogravimetric analysis of PPy and doped PPy thin film

processes. The initial stages of weight loss at 100 °C could be due to the vaporization of water molecules and oligomers as well as elimination of unreacted monomer [33]. At 200 °C, the protonic acid component of the polymer is lost, and finally, at 300–600 °C the decomposition of polymer chain occurs, which leads to the production of volatile gases [33]. Henceforth, PPy and doped PPy are stable up to 200 °C.

## Photoluminescence

It is widely accepted that  $\pi \rightarrow \pi^*$  electronic transitions in the polymeric units play a key role in the PL emission of PPy thin film. Owing to the presence of conjugated double bonds in the products, we studied the PL properties of the PPy and doped PPy thin film. Figure 9 shows the room-temperature PL spectra of the thin films excited at 325 nm. All the samples exhibit blue luminescence properties similar to other PPy reported [34] earlier. The spectra show broad peaks centred at 425 and 480 nm for PPy and doped PPy thin film, respectively. This transition may be due to polaron and bipolaron transition [35]. Son et al. [36] reported similar type of PL intensity. In our present study, a lower PI intensity of NaI-PPy thin film is observed, which indicates higher electron–hole pair separation efficiency. So this material can be a potential candidate for photocatalysis.

## Electrical conductivity

From the measured  $I$ – $V$  characteristics of PPy and doped PPy thin films, the values of electrical conductivities have been obtained by using the equation

$$\sigma = [(I \times L) / (V \times A)] \quad (5)$$

where  $I$  is the current,  $V$  is the voltage,  $L$  is the thickness of pellet and  $A$  is the cross-sectional area of the pellet.

Table 2 shows the conductivity of PPy and doped PPy thin films. The conductivity decreases in the order  $\sigma(\text{NaI-PPy}) > \sigma(\text{C2-PPy}) > \sigma(\text{C1-PPy}) > \sigma(\text{TSA-PPy}) > \sigma(\text{DBSA-PPy}) > \sigma(\text{HCl-PPy}) > \sigma(\text{PPy})$ . Polarons and bipolarons are dominant charge carriers, which are responsible for the electrical conduction in these thin film

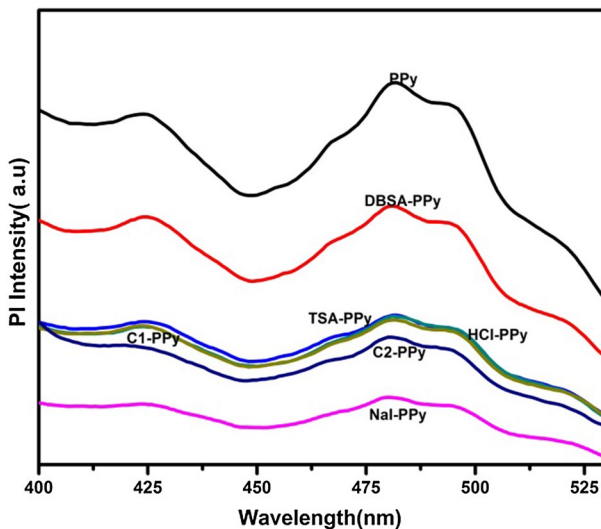


Fig. 9 Photoluminescence of PPy and doped PPy thin film

**Table 2** Electrical properties for PPy and doped PPy thin film

Polymer	Bulk concentration ( $\text{cm}^{-3}$ )	Sheet concn ( $\text{cm}^{-2}$ )	Conductivity ( $\Omega^{-1} \text{cm}^{-1}$ )	Mobility unit ( $\text{cm}^2/\text{Vs}$ )	Average Hall coef- ficient ( $\text{cm}^3/\text{C}$ )	Band gap (eV)
PPy	$1.4689 \times 10^{14}$	$1.4689 \times 10^{11}$	$5.0004 \times 10^{-5}$	2.125	$4.2495 \times 10^4$	2.3261
DBSA-PPy	$4.7531 \times 10^{13}$	$4.7531 \times 10^{10}$	$5.0418 \times 10^{-4}$	$6.6213 \times 10^1$	$1.3133 \times 10^5$	2.1150
TSA-PPy	$8.8511 \times 10^{13}$	$8.8511 \times 10^{10}$	$2.3527 \times 10^{-4}$	$1.6592 \times 10^1$	$7.0524 \times 10^4$	1.93
HCl-PPy	$5.8507 \times 10^{13}$	$5.8507 \times 10^{10}$	$7.4447 \times 10^{-4}$	$4.797 \times 10^2$	$1.0669 \times 10^5$	1.96
NaI-PPy	$1.4847 \times 10^{14}$	$1.4847 \times 10^{11}$	$6.7514 \times 10^{-2}$	$2.8385 \times 10^3$	$4.2043 \times 10^4$	1.75
C1-PPy	$4.2355 \times 10^{13}$	$4.2355 \times 10^{10}$	$4.4962 \times 10^{-3}$	$1.0972 \times 10^2$	$1.4738 \times 10^5$	1.86
C2-PPy	$4.3082 \times 10^{13}$	$4.3082 \times 10^{13}$	$4.3018 \times 10^{-3}$	$6.2329 \times 10^2$	$1.4489 \times 10^5$	1.81

samples. As the strength of the applied field increases, the number of such polarons and bipolarons increases, resulting in the increment of current [37]. This results in an increase in conductivity with voltage as more and more number of polarons and bipolarons are available in the system. Doping causes bond change from aromatic configuration to quinoid configuration, which is higher in energy and confines the charge and spin density to a self-localized structural deformation that is mobile along the chain [38].

In our present study, TSA-PPy shows higher conductivity than DBSA-PPy because of small band gap and small alkyl group. Citric acid has effective conjugation lengths due to three carboxylic acids present in citric acid and short alkyl chain which contributes to higher conductivity. C2-PPy shows higher conductivity than C1-PPy. Apart from citric acid, *citrus lemon* contains terpenes, tannins, reducing sugar and polyphenol, which is responsible for the increase in conductivity.

The synthesized NaI-PPy thin film showed 1000 times higher conductivity than PPy thin film and also exhibited higher conductivity when compared to all other doped PPy. The higher conductivity is due to an increase in mobility of NaI as well as a decrease in band gap as given in Table 2. The smaller value of optical band gap energy allows easy  $\pi-\pi^*$  electronic transition and hence results in higher value of electrical conductivity. Khanmirzaei et al. [39] reported that an increase in ionic conductivity in starch-based polymer electrolytes is due to an increase in mobile ions of iodide salts in the systems. Singh [40] synthesized potassium iodide-doped biopolymer electrolyte and found an increase in ionic conductivity due to mobile charge carriers of  $K^+$  and  $I^-$  ions. Shirwa et al. [41] also proved higher conductivity of polyacetylene doped with NaI due to charge transfer mechanism. From the results of our present study, it was concluded that the high electrical conductivity of NaI-PPy thin film is due to low band gap, high mobility and charge transfer mechanism and suggests the presence of deep localized state in the band gaps.

Navale [31] has reported electrical conductivity of 50% camphor sulphonic acid-doped polypyrrole thin film synthesized by casting method exhibited  $1.56 \times 10^{-8}$  S/cm. The electrical conductivity of PPy thin film synthesized via inkjet printing method revealed  $1.5 \times 10^{-6}$  S/cm [42]. So therefore we argue that our NaI-PPy thin film exhibited electrical conductivity of  $6.75 \times 10^{-2}$  S/cm which is much higher than reported in the literature.

### Photocatalytic performance of PPy thin film

Waste waters generated by the textile industries contain considerable amounts of non-fixed dyes and especially of azo dyes which are toxic to aquatic life and create serious environmental pollution. Rhodamine 6G (an azo dye) is a fairly stable and persistent dye pollutant under visible-light irradiation. In our present study, NaI-PPy thin film has low band gap and higher conductivity when compared to other doped PPy thin film. So this material was chosen for the photocatalytic activity of rhodamine 6G (R6G) (taken as model pollutants) in water under visible light.

Figure 10 depicts UV–Vis spectrum of R6G during photoirradiation with NaI-PPy catalyst with various time intervals. The R6G shows major absorption peaks in

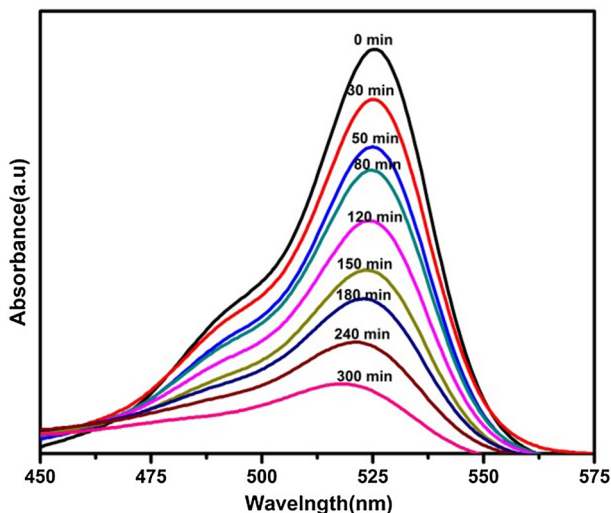


**Fig. 10** Absorbance spectra of rhodamine 6G during the course of reaction

visible region at 524 nm. R6G shows main absorption peaks at 524 nm in the visible region. The rate of decolorization was recorded with respect to the change in intensity of absorption peaks at 524 nm for R6G. The absorption peaks, corresponding to dye, diminished and finally disappeared during reaction, which indicated that the dye had been degraded.

The concentration of R6G is 5 mg/L ( $10.4379 \times 10^{-6}$  M) catalyst dose (1 cm  $\times$  1 cm) thin film, and duration is 3 h. The obtained degradation curves of R6G dye are shown in Fig. 11. NaI-PPy thin film exhibited a visible light-induced photocatalytic activity with 76% degradation of R6G dye after long irradiation (300 min). However, only 51% degradation has been achieved for PPy thin film under identical reaction conditions. NaI-PPy thin film exhibited the highest catalytic activity with a 25% increase in degradation efficiency.

Tinacaba et al. [43] reported degradation rate of 1.37%/min for  $2.56 \times 10^{-6}$  M of R6G dye using ZnO/Zn thin film in UV light. The degradation efficiency in the present technique is the same as reported by Tinacaba, but in our case we used visible light for dye degradation. The better efficiency of thin film catalyst is due to the absorption of light by the catalyst from UV to visible part of the spectrum. The number of photons available in artificial UV light and artificial visible light is  $80.49 \times 10^{20}$  photon/s and  $4.15 \times 10^{20}$  photon/s, respectively. So in our present system, the dye degradation efficiency is better with lesser number of photons itself compared to UV light [43]. Our results are better than other reported rates such as by Kansal et al. [44] wherein it took 180 min to degrade 200 mg/l rhodamine 6G dye by 20% for a ZnO catalyst dose of 0.5 g/l. Compared with the literature, we have reached a better degradation efficiency in visible light.

The results showed that both films are effective in producing electron–hole pairs that can degrade organic materials. One of the key features of a photocatalyst is that

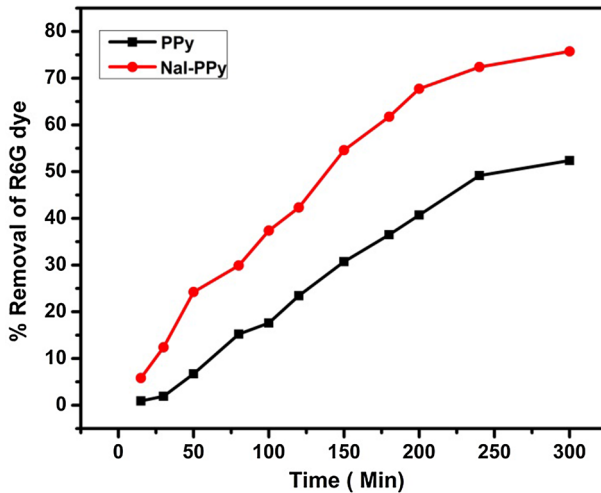


**Fig. 11** Effect of time variation on the photodegradation of R6G dye on PPy and NaI-PPy thin film

it must be efficiently recycled and reused after repeating cycles of degradation reactions. As the PPy is in thin film form, it could be efficiently recycled and reused for repeating cycles without appreciable loss of activity, which promotes the NaI-PPy thin film photocatalyst for its practical applications in the field of environmental protection.

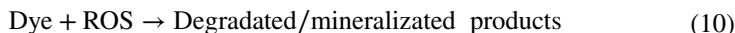
Photocatalysis involves generation of charge carriers, i.e. excess electrons ( $e^-$ ) and holes ( $h^+$ ), and the catalytic reactions induced by these species. NaI-PPy has higher electrical conductivity, which implies more charge carriers are available in the system for efficient photocatalytic degradation of dyes. A high photocatalytic activity is closely related to an efficient separation of the photoexcited electron–hole pairs generated in the photocatalyst after its excitation. The organic pollutants and dyes can be photodegraded via a photocatalytic oxidation process. A large number of major reactive species including holes,  $HO^\cdot$  and  $O_2^{\cdot-}$  radicals are involved in the photocatalytic oxidation process. A mechanism was proposed by Ghosh et al. [45] for the photoactivity of poly(3,4-ethylenedioxythiophene) (PEDOT) under visible light. In our present study, a similar mechanism was proposed.

In our present study, due to low band gap of the NaI-PPy, less energy is required to promote an electron to the conduction band and as a result more electronic transitions are likely to occur at higher wavelength radiation (less energetic) compared with PPy. Under visible-light irradiation, a photon excites an electron from the valence band (VB) to the conduction band (CB) of NaI-PPy. Hence, the electrons can easily migrate into the surface of the NaI-PPy and react with oxygen to form oxidizing  $O_2^{\cdot-}$  superoxide radical. This effective separation of photogenerated electron–hole thereby promotes enhanced photocatalytic activity. Sarbanti Ghosh et al. [45] proposed mechanism for the formation of  $HO^\cdot$  radicals (Eqs. 6–9):





The results show that the photocatalysis mechanism involves  $\text{O}_2^-$ , photoinduced  $\text{h}^+$  and  $\text{HO} \cdot$  radicals mediated degradation of organic pollutant with effective charge separation in NaI-PPy thin film. The overall reaction of dye photodegradation can be resumed as follows [46]:



When the reaction order for such photodegradation obeys the pseudo-first-order kinetics, the following equation can be used:

$$-dC/dt = kC \quad (11)$$

where  $t$  represents the photodegradation time and  $k$  is the observed pseudo-first-order rate constant. By integrating Eq. (11), the following expression is obtained:

$$-\ln C/C_0 = kt \quad (12)$$

Thus, a plot of  $-\ln(C/C_0)$  vs. time leads to a linear diagram which slope equals the observed pseudo-first-order rate constant of photodegradation [47]. Figure 12 shows a plot of  $-\ln(C/C_0)$  vs. time in which it can be observed that all photodegradation followed pseudo-first-order kinetics, indicating that the photodegradation rate is directly proportional to R6G concentration. The  $k$  value using thin film and 5 mg/L of initial R6G concentration for the NaI-PPy thin film was two times higher ( $k=0.00586 \text{ min}^{-1}$ ) than that using PPy thin film ( $k=0.00281 \text{ min}^{-1}$ ).

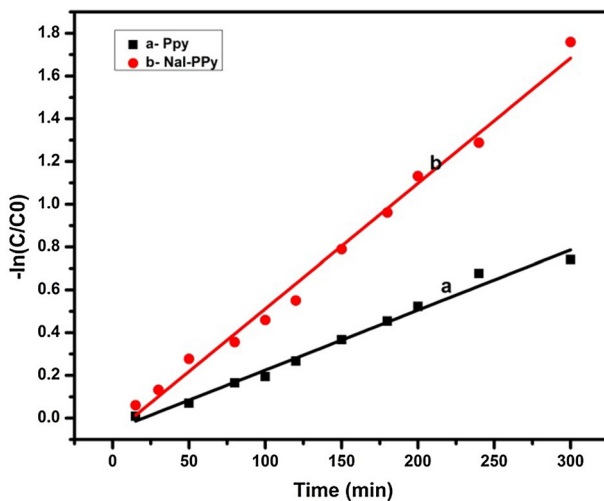


**Fig. 12**  $-\ln(C/C_0)$  as a function of time throughout R6G dye photodegradation under visible-light irradiation using PPy and NaI-PPy thin film



Low band gap and high conductivity are responsible for higher photocatalytic activity in NaI-PPy thin film. A lower PL intensity of NaI-PPy thin film indicates higher electron–hole pair separation efficiency, which is also responsible for the fast degradation rate of R6G dye. So this material can also be employed as a candidate for hybrid solar cell application.

## Conclusion

In summary, PPy and doped PPy thin film has been synthesized by a facile and reproducible SILAR method at room temperature. The NaI-PPy thin film with much narrower band gap (1.75 eV) compared with other doped PPy thin film has therefore excellent ability to absorb light in visible regions. Our results demonstrate that NaI-PPy thin film shows exceptional high photocatalytic activities under visible light and is of huge potential for environmental remediation. The photocatalytic oxidation reactions involve the oxidative  $O_2^-$  and  $HO^\cdot$  species. Our results demonstrate that conducting polymers constitute a new class of photocatalysts for environment remediation. The catalyst can be reusable, scalable and capable of functioning in visible light, which is especially important in the degradation of dyes. As NaI-PPy thin film exhibits a wide range of absorption, low band gap and better electron hole separation efficiency, it can also serve as better candidate for hybrid solar cell application.

**Acknowledgements** This work is mainly supported by the research funds from the management of Hindustan University through CENCON. Authors also acknowledge research funding from Dongguk University through QSRC and NITA. This research was also supported by Leading Foreign Institute Recruitment Program through the National Research Foundation of Korea (NRF) funded by the Ministry of Education Science and Technology (MEST) (No. 2013-044975) and by the International Research and Development Program of the National Research Foundation of Korea (NRF) funded by the Ministry of Education, Science and Technology (MEST) of Korea (Grant Number: 2012-033431).

## References

1. Chu S, Majumdar A (2012) Opportunities and challenges for a sustainable energy future. *Nature* 488:294–303
2. Chen X, Li C, Grätzel M, Kostecki R, Mao SS (2012) Nanomaterials for renewable energy production and storage. *Chem Soc Rev* 41:7909–7937
3. Zhang Q, Uchaker E, Candelaria SL, Cao G (2013) Nanomaterials for energy conversion and storage. *Chem Soc Rev* 42:3127–3171
4. Asahi R, Morikawa T, Ohwaki T, Aoki K, Taga Y (2001) Visible-light photocatalysis in nitrogen-doped titanium oxides. *Science* 293:269–271
5. Schneider J, Matsuoka M, Takeuchi M, Zhang J, Horiuchi Y, Anpo M, Bahnemann D (2014) Understanding  $TiO_2$  photocatalysis: mechanisms and materials. *J Chem Rev* 114:9919–9986
6. Xu X, Randorn C, Efstathiou P, Irvine JTS (2012) A red metallic oxide photocatalyst. *Nat Mater* 11:595–598
7. Liu L, Ouyang S, Ye J (2013) Gold-nanorod-photosensitized titanium dioxide with wide-range visible-light harvesting based on localized surface plasmon resonance. *Angew Chem Int Ed* 52:6689–6694
8. Zhang N, Zhang Y, Xu J (2012) Recent progress on graphene-based photocatalysts: current status and future perspectives. *Nanoscale* 4:5792–5813

9. Li L, Yan J, Wang T, Zhao Z, Zhang J, Gong J, Guan N (2015) Sub-10 nm rutile titanium dioxide nanoparticles for efficient visible-light-driven photocatalytic hydrogen production. *Nat Commun* 6:5881–5891
10. Tao J, Luttrell T, Batzill M (2011) A two-dimensional phase of TiO<sub>2</sub> with a reduced bandgap. *Nat Chem* 3:296–300
11. Chen XB, Liu L, Yu PY, Mao SS (2011) Increasing solar absorption for photocatalysis with black hydrogenated titanium dioxide nanocrystals. *Science* 331:746–750
12. Linic S, Christopher P, Ingram DB (2001) Plasmonic-metal nanostructures for efficient conversion of solar to chemical energy. *Nat Mater* 10:911–921
13. Weng L, Zhang H, Govorov AO, Ouyang M (2014) Hierarchical synthesis of non-centrosymmetric hybrid nanostructures and enabled plasmon-driven photocatalysis. *Nat Commun* 5:4792–4802
14. Grabowska E, Zaleska A, Sorgues S, Kunst M, Etcheberry A, Colbeau-Justin C, Remita H (2013) Modification of titanium(IV) dioxide with small silver nanoparticles: application in photocatalysis. *J Phys Chem C* 117:1955–1962
15. Hai Z, Kolli N, Uribe D, Beauvier P, Yacaman M, Vigneron J, Etcheberry A, Sorgues S, Justin C, Chen J, Remita H (2013) Modification of TiO<sub>2</sub> by bimetallic Au–Cu nanoparticles for wastewater treatment. *J Mater Chem A* 1:10829–10836
16. Kowalska E, Yoshiiri K, Wei Z, Zheng S, Kastl E, Remita H, Ohtani B, Rau S (2015) Hybrid photocatalysts composed of titania modified with plasmonic nanoparticles and ruthenium complexes for decomposition of organic compounds. *Appl Catal B Environ* 178:133–143
17. Naik GV, Shalaev VM, Boltasseva A (2013) Alternative plasmonic materials: beyond gold and silver. *Adv Mater* 25:3264–3294
18. Ghosh S, Kouame N, Remita S, Goubard F, Aubert P, Dazzi A, Besseau A, Remita H (2015) Conducting polymer nanostructures for photocatalysis under visible light. *Nat Mater* 14:505–510
19. Khodagholy T, Doublet P, Quilichini M, Gurfinkel P, Leleux A, Ghestem E, Ismailova T, Hervé S, Sanaur C Bernard, Malliaras G (2013) In vivo recordings of brain activity using organic transistors. *Nat Commun* 4:1575–1582
20. Li G, Shrotriya V, Huang J, Yao Y, Moriarty T, Emery K, Yang Yang (2005) High-efficiency solution processable polymer photovoltaic cells by self-organization of polymer blends. *Nat Mater* 4:864–868
21. Cai M, Ye Z, Xiao T, Liu R, Chen Y, Mayer R, Biswas R, Ho K, Shinar R, Shinar J (2012) Extremely efficient indium–tin-oxide-free green phosphorescent organic light-emitting diodes. *Adv Mater* 24:4337–4342
22. Muktha B, Madras G, Guru Row U, Patil S (2007) Conjugated polymers for photocatalysis. *J Phys Chem B* 111:7994–7998
23. Alam P, Alam A, Anwer MdK, Alqasoumi S (2014) Quantitative estimation of hesperidin by HPTLC in different varieties of citrus peels. *Asian Pac J Trop Biomed* 4(4):262–266
24. Rauf A, Uddin G, Ali J (2014) Phytochemical analysis and radical scavenging profile of juices of *Citrus sinensis*, *Citrus anrantifolia*, and *Citrus limonum*. *Organ Med Chem Lett* 4:5–8
25. Wang ZL, Kong XY, Ding Y, Gao P, Hughes WL, Yang R, Zhang Y (2004) Semiconducting and piezoelectric oxide nanostructures induced by polar surfaces. *Adv Func Mater* 14:943–956
26. Shiigi H, Kishimoto M, Yakabe H, Deore B, Nagaoka T (2002) Highly selective molecularly imprinted overoxidized polypyrrole colloids one-step preparation technique. *Anal Sci* 18:41–45
27. Song MK, Kim YT, Kim BS, Kim J, Char K, Rhee HW (2004) Synthesis and characterization of soluble polypyrrole doped with alkylbenzenesulfonic acids. *Synth Met* 141:315–319
28. Hazarika J, Kumar A (2016) Studies of structural, optical, dielectric relaxation and ac conductivity of different alkylbenzenesulfonic acids doped polypyrrole nanofibers. *Physica B Condens Matter* 481:268–279
29. Chen L, Wang K, Mahmoud SM, Li Y, Huang H et al (2015) Effects of replacing thiophene with 5,5-dimethylcyclopentadiene in alternating poly(phenylene), poly(3-hexylthiophene), and poly(fluorene) copolymer derivatives. *Polym Chem* 6:7533–7542
30. Navale ST, Mane AT, Ghanwat AA, Mulik AR, Patil VB (2014) Camphor sulfonic acid (CSA) doped polypyrrole (PPy) films: measurement of microstructural and optoelectronic properties. *Measurement* 50:363–369
31. Arora K, Chaubey A, Singhal R, Singh RP et al (2006) Application of electrochemically prepared polypyrrole-polyvinyl sulphonate films to DNA biosensor. *Biosens Bioelectron* 21:1777–1783
32. Wang G, NeoH KG, Kang ET (2004) Comparative study of chemically synthesized and plasma polymerized pyrrole and thiophene thin films. *Thin Solid Films* 446:205–217

33. Jayamurgan P, Ponnuswamy V, Ashokan S, Mahalingam T (2013) The effect of dopant on structural, thermal and morphological properties of DBSA-doped polypyrrole. *Iran Polym J* 22:219–225
34. Galář B, Dzurňák P, Malý J, Čermák A, Kromka M, Omastová B, Rezek (2013) Chemical changes and photoluminescence properties of UV modified polypyrrole. *Int J Electrochem Sci* 8:57–70
35. Jang KS, Ko HC, Moon B, Lee H (2005) Observation of photoluminescence in polypyrrole micelles. *Synth Met* 150:127–131
36. Son AJR, Lee H, Moon B (2007) Morphology and photoluminescence of colloidal polypyrrole nanoparticles. *Synth Met* 157:597–602
37. Shaktawat V, Jain N, Saxena R, Saxena NS, Sharma TP (2006) Electrical conductivity and optical band gap studies of polypyrrole doped with different acids. *Polym Bull* 57:535–542
38. Naveen Kumar M, Nagabhooshanam M, Anand Rao M, Bhagvanth Rao M (2001) Preparation and characterization of doped polybenzidine. *Cryst Res Technol* 36:309–317
39. Khanmirzaei MH, Ramesh S, Ramesh K (2015) Effect of different iodide salts on ionic conductivity and structural and thermal behavior of rice-starch-based polymer electrolytes for dye-sensitized solar cell application. *Ionics* 21:2383–2391
40. Singh R, Baghel J, Shukla S, Bhattacharya B, Rhee H-W, Singh PK (2014) Detailed electrical measurements on sago starch biopolymer solid electrolyte. *Phase Transit* 87:1237–1245
41. Sirakawa H, Louis EJ, Macdiarmid AG, Chiang CK, Heeger AJ (1977) Synthesis of electrically conducting organic polymers: halogen derivatives of polyacetylene, (CH)<sub>x</sub>. *J Chem Soc, Chem Commun* 16:578–580
42. Mabrook MF, Pearson C, Petty MC (2006) Inkjet-printed polypyrrole thin films for vapour sensing. *Sens Actuators, B* 115:547–551
43. Tinacba EJC, Nuñez JA, Tumlos RB, Ramo HJ (2016) ZnO/Zn and ZnO film deposited via microwave atmospheric plasma jet as photo-catalyst for Rhodamine 6G dye degradation. *Thin Solid Films*. <https://doi.org/10.1016/j.tsf.2016.07.01>
44. Kansal SK, Singh M, Sud D (2007) Studies on photodegradation of two commercial dyes in aqueous phase using different photocatalysts. *J Hazard Mater* 141:581–590
45. Ghosh S, Kouame N, Remita S, Ramos L, Goubard F, Aubert P, Dazzi A, Deniset-Besseau A, Remita H (2015) Visible-light active conducting polymer nanostructures with superior photocatalytic activity. *Sci Rep* 5:18002–18011
46. Ovando-Medina VM, López RG, Castillo-Reyes BE, Alonso-Dávila PA, Martínez-Gutiérrez H, González-Ortega O, Fariás-Cepeda L (2015) Composite of acicular rod-like ZnO nanoparticles and semiconducting polypyrrole photoactive under visible light irradiation for methylene blue dye photodegradation. *Colloid Polym Sci* 293:3459–3469
47. Montazerzohori M, Nasr-Esfahani M, Joohari S (2012) Iron and aluminium based adsorption strategies for removing arsenic from water. *Environ Prot Eng* 38:45–56